Excitation profiles of resonance electronic Raman scattering in $ErPO_4$ crystals

G. M. Williams,* P. C. Becker,† and N. Edelstein
Department of Physics, University of California, Berkeley, California 94720
and Materials and Chemical Sciences Division, Lawrence Berkeley Laboratory, 1 Cyclotron Road, Berkeley, California 94720

L. A. Boatner and M. M. Abraham
Solid State Division, Oak Ridge National Laboratory, P.O. Box 2008, Oak Ridge, Tennessee 37831-6032
(Received 13 March 1989)

The intensities of electronic Raman-scattering transitions between the ground and excited crystal-field states of the ground $^4I_{15/2}$ multiplet of Er^{3+} in crystals $ErPO_4$ were measured as a function of excitation frequency in the region of an intermediate-state resonance between the $^4I_{15/2}$ ground state and a crystal-field state of the $^4F_{7/2}$ multiplet. It is shown that for excitation frequencies near the intermediate-state resonance, the observed spectra are the result of electronic Raman scattering and are not due to absorption followed by fluorescence. No such determination could be made for direct resonance excitation. Enhancements of the intensities of the electronic Raman scattering by a factor on the order of 100 are reported. The electronic Raman-scattering excitation profiles (excitation frequency versus enhancement) are found to be asymmetric in excitation frequency about the resonance. These profiles can be accurately modeled using standard electronic Raman intensity theory and the measured oscillator strengths and linewidths of the $^4I_{15/2} \rightarrow {}^4F_{7/12}$ one photon transitions.

I. INTRODUCTION

Resonance enhancements of the intensities of electronic Raman-scattering transitions between crystal-field levels of the ground $^4I_{15/2}$ multiplet of $Er^{3+}(4f^{11})$ in erbium-doped phosphate crystals have been reported previously.[1] These enhancements were observed using the 488.0-nm line of an argon-ion laser that is nearly coincident in frequency with transitions between the crystal-field levels of the $^4I_{15/2}$ and $^4F_{7/2}$ multiplets. The previous results were unusual in that the intensity enhancements were anomalously large (by a factor on the order of 10–100). Such intraconfigurational resonances should generally be small since they are dependent on $4f^N$-$4f^N$ electric dipole matrix elements that are formally parity forbidden. Additionally, other earlier experiments involving $4f^N$-$4f^N$ enhancements of electronic Raman scattering resulted in observed enhancements of factors of only 1–5 in intensity.[2–4]

This paper presents new results obtained by varying the frequency of the exciting light. The present results confirm that the observed spectra are due to electronic Raman scattering and are not due to fluorescence. In addition, excitation profiles for the resonance enhancement of the electronic Raman scattering were obtained, and the results are modeled using data obtained from $^4I_{15/2} \rightarrow {}^4F_{7/2}$ absorption measurements. A striking feature of the data is the observed asymmetry in the excitation profile about the resonance—a feature that is attributed to interference between nonresonant and resonant scattering amplitudes.

A general understanding of resonances of this type is useful in analyzing the resonant enhancement of other inherently weak multiphoton processes such as two-photon absorption and four-wave mixing. Recently, Cone and co-workers have reported intermediate-state resonances for four-wave mixing in crystals of $Tb(OH)_3$ and $LiTbF_4$,[5–9] and an intermediate-state resonance enhancement of a factor of 20 for two-photon absorption in crystals of Tb^{3+}:$LiYF_4$.[10]

II. EXPERIMENT

Experiments were performed on single crystals of $ErPO_4$ whose preparation and characteristics have been described previously.[11] A schematic of the experimental setup is shown in Fig. 1, where the laser-excitation source was a Quanta-Ray PDL-1 dye laser (Coumarin-500 dye) which was pumped by the frequency-tripled output of a Quanta-Ray DCR-1 Q-switched neodymium-doped yttrium aluminum garnet (Nd:YAG) laser. This system produced laser light with a temporal width of ~ 10 ns and a spectral width of ~ 0.25 cm^{-1}. The main source of background signal in the experiment was amplified spontaneous emission (ASE) from the dye laser. Since ASE generates a signal across the entire gain curve of the dye, the dye-laser output was spectrally filtered to reduce this background signal using a 0.25-m Jobin-Yvon monochromator with a bandpass of approximately 15 cm^{-1} in the range of interest. A small portion of the beam was sampled by a silicon photodiode for normalization purposes.

All experiments were carried out with the sample mounted on the cold finger of a Janis cyrostat and kept at a temperature of approximately 10–15 K. The scattered light was collected at 90° by a fast camera lens and was spectrally analyzed using a Spex Industries 1403 double

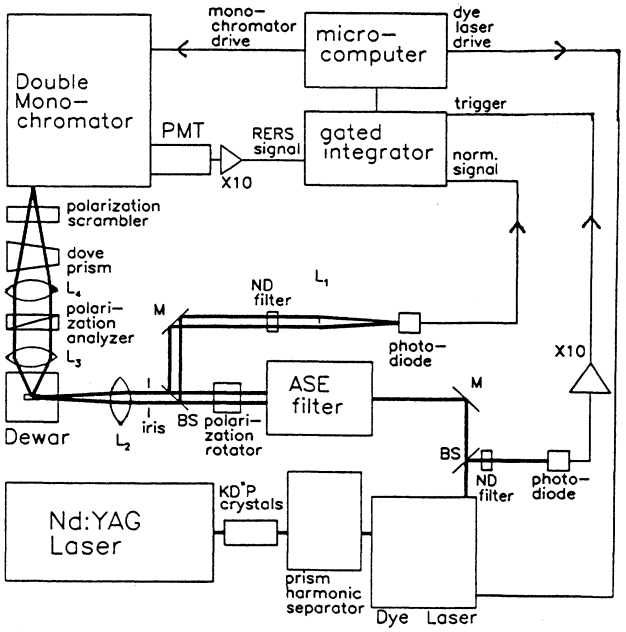

FIG. 1. Experimental setup for obtaining resonance electronic Raman-scattering spectra. The ASE filter consists of a 0.25-m Jobin-Yvon monochromator and associated lens. See Ref. 19 for a more complete description.

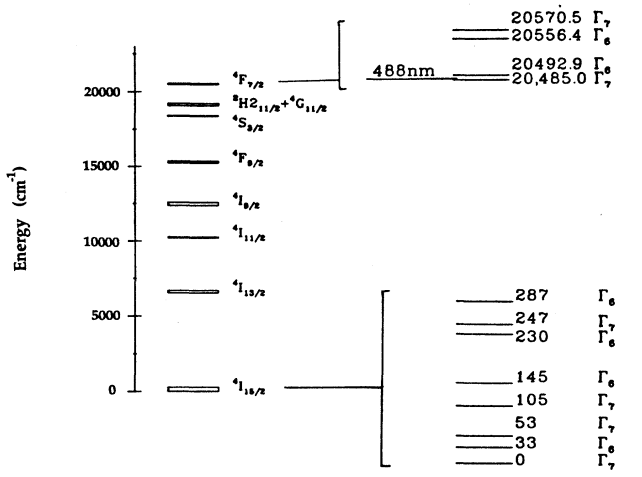

FIG. 2. Electron structure of Er^{3+} in $ErPO_4$. The crystal-field levels from the $^4I_{15/2}$ and $^4F_{7/2}$ multiplets are shown on the right side of the figure.

monochromator. A RCA 31034 cooled photomultiplier tube (PMT) was used for the photon detector. The PMT signal was amplified by a fast LeCroy 101B×10 current amplifier. The PMT signal and the photodiode signal were fed into two SRI-250 boxcar integrators for gated detection. These integrators were used as sample-and-hold devices and the shot-to-shot information was digitized and stored using a Digital Equipment Corporation (DEC) LSI-11/2 microcomputer. The LSI-11/2 microcomputer performed shot-to-shot normalization, averaging, and also controlled the scanning of the dye laser and collection spectrometer synchronously.

The intensities of the Raman transitions excited by the pulsed dye laser and/or argon-ion laser were compared by normalizing the measured intensities to the intensity of the vibrational Raman transition of $ErPO_4$ at 303 and/or 1026 cm^{-1}.

III. ELECTRONIC STRUCTURE

Er^{3+} has a ground electronic configuration $[Xe]4f^{11}$ that is split by the Coulomb and spin-orbit interactions into a number of multiplets with different energies. For energies up to 21 000 cm^{-1}, the multiplet structure of Er^{3+} is shown in Fig. 2, where the multiplets are labeled by the leading Russell-Saunders term(s) ($^{2S+1}L_J$) of their wave functions. The crystal field of $ErPO_4$ splits these multiplets, and individual crystal-field levels of the $^4I_{15/2}$ and $^4F_{7/2}$ multiplets for Er^{3+} in $ErPO_4$ are also shown in Fig. 2. These levels are labeled by the double-group irreducible representations (Γ_6 and Γ_7) of the D_{2d} point group that describes the symmetry of Er^{3+} sites in $ErPO_4$. All of the crystal-field states are doubly degenerate Kramers pairs. In Fig. 2 the energy of the 488-nm (20 486.7 cm^{-1} in vacuum) line of the argon-ion laser used in the earlier work is also displayed. The near resonance of this line with the transition between the ground state and the lower two crystal-field levels of the $^4F_{7/2}$ multiplet (i.e., 20 485.0 and 20 492.9 cm^{-1}) is clearly evident.

In this work, the intensities of the electronic Raman-scattering transition from the ground state to crystal-field levels of the multiplet $^4I_{15/2}$ at 33 and 53 cm^{-1} were measured as a function of laser-excitation frequency. Incident-laser-excitation frequencies were selected to be in near coincidence with transitions from the ground state to the lower two crystal-field levels of the $^4F_{7/2}$ multiplet. To simplify the analysis of the experiment, the polarizations of the incident and scattered light were selected such that, through the D_{2d} crystal-field electric dipole selection rules, only resonance with the level at 20 492.7 cm^{-1} was allowed. Polarization of the exciting laser light was selected parallel to the optical axis of the crystal ($\hat{Z}$), while the scattered-light polarization was selected parallel to one of the two equivalent axes of the crystal ($\hat{X}$). This Raman geometry is labeled as $\hat{Y}(\hat{X}\hat{Z})\hat{X}$ (where the $\hat{X}$ and $\hat{Y}$ signify the incident and scattered light directions, respectively).

IV. DISCRIMINATION BETWEEN FLUORESCENCE AND RESONANCE RAMAN SCATTERING

In performing electronic Raman-scattering experiments in rare-earth crystals, care must be taken to ensure that the observed signals are indeed Raman-scattered light and not simplify fluorescence from a populated excited state. This is especially true for cases in which the exciting laser frequency is in resonance or near resonance with an electronic transition in the crystal. In such cases, not only is a population of the excited states more likely (thus facilitating fluorescence), but also discrimination of

the Raman and fluorescence signals becomes more difficult since the two signals are expected at approximately the same frequencies.

In the previously reported work on $ErPO_4$,[1] careful measurements of the frequencies of the observed signals indicated that the spectra were the result of resonance-enhanced electronic Raman scattering to the levels at 33 and 53 cm^{-1}. This determination was possible because the 488-nm line of the argon-ion laser was not in exact resonance with any electronic transitions (see Fig. 2). Thus the fluorescence and Raman transitions were expected at slightly different frequencies.

To confirm the above finding, an $ErPO_4$ crystal was excited at a number of energies in the region of 20490 cm^{-1}. Spectra associated with the different laser excitation frequencies are shown in Fig. 3. The horizontal axis represents the frequency shift in cm^{-1} from the laser-excitation frequency. In such a plot, Raman-scattered light should appear in the same position regardless of the laser-excitation frequency, while the position of fluorescence peaks will change with excitation frequency. A plot of the measured frequency shifts of the observed spectral peaks relative to the laser-excitation frequency is shown in Fig. 4 as a function of laser-excitation frequency. This plot also includes data from additional spectra not shown in Fig. 3. The horizontal lines give expected locations of spectral peaks resulting from Raman transitions from the ground state to the 33- and 53-cm^{-1} levels, while the skewed lines show expected locations of peaks resulting from fluorescence transitions from the level at 20492.9 cm^{-1} to the levels at 33 and 53 cm^{-1}. The data show that for excitation frequencies that are not in direct resonance with the transition 0 $cm^{-1} \rightarrow 20492.9$ cm^{-1}, the observed spectra derive from the Raman-scattering transitions 0 $cm^{-1} \rightarrow 33$ cm^{-1} and 0 $cm^{-1} \rightarrow 53$ cm^{-1}. In fact, in the spectra shown in Fig. 3 there is no indication of any fluorescence peaks.

For excitation frequencies very near the energy of the resonant transition, the discrimination between resonance Raman scattering and fluorescence is not straightforward. This is due not only to the experimental limitations in measuring frequency shifts (± 0.5 cm^{-1}), but also to the nonzero linewidth of the resonant transition. In this case, the resonant transition has a full width at half maximum (FWHM) of approximately 2.0 cm^{-1}. If this broadening is assumed to be inhomogeneous (i.e., resulting from Er^{3+}-site variations), it is possible that for excitation frequencies within the linewidth of the resonant transition, site-selective fluorescence and resonant Raman scattering would occur at the same frequency. For this to occur, however, the energy difference between the initial and final states of the Raman and/or fluorescence process has to be site independent. This seems unlikely given that the nonresonantly excited 0 $cm^{-1} \rightarrow 33$ cm^{-1} and 0 $cm^{-1} \rightarrow 53$ cm^{-1} Raman-scattering transitions have finite linewidths. Both of these scattering transitions have a FWHM of approximately 2.0 cm^{-1}.[12] If this broadening is inhomogeneous, then the energy difference between the initial and final states is site dependent.

Another observation indicates that, for excitation fre-

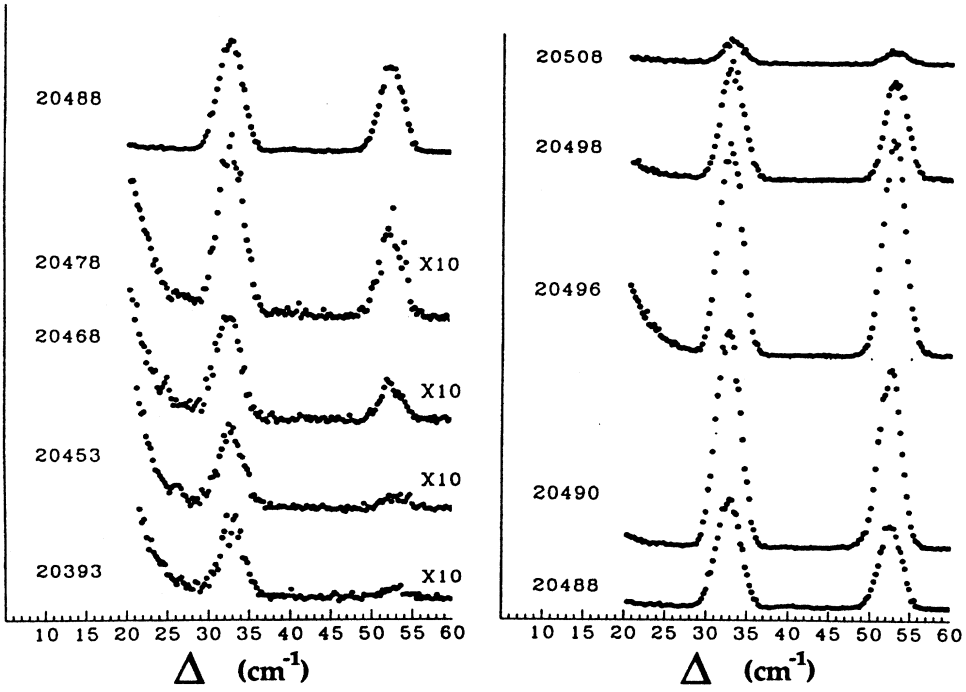

FIG. 3. $\hat{Y}(\hat{X}\hat{Z})\hat{X}$ Raman spectra of $ErPO_4$ excited using different photon energies. The horizontal axis represents the shift from the labeled excitation energies.

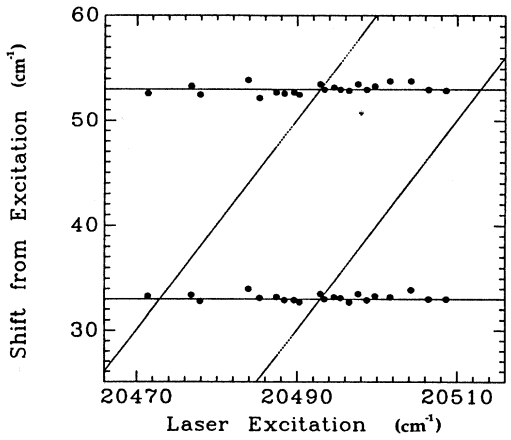

FIG. 4. Frequency shifts of the peaks in the $\hat{Y}(\hat{X}\hat{Z})\hat{X}$ spectra of $ErPO_4$ as a function of excitation frequency. The horizontal lines are expected locations of Raman peaks. The skewed lines are expected locations of fluorescence peaks.

quencies within the resonant-transition linewidth, the observed spectra result from resonant Raman scattering and not site-selective fluorescence. Fluorescence from the transitions 20 492.9 $cm^{-1} \rightarrow 33$ cm^{-1} and 20 492.9 $cm^{-1} \rightarrow 53$ cm^{-1}, excited by populating either the upper levels of the $^4F_{7/2}$ multiplet or higher-energy multiplets,[1] is quenched by nonradiative decay and is very weak. Conversely, the signals emitted after excitation in the region of 20 490 cm^{-1} are orders of magnitude stronger.

Several experiments have been reported that discriminate between fluorescence and resonance Raman scattering by lifetime measurements.[3,13–15] The fluorescence is expected to have a lifetime equivalent to the population or longitudinal lifetime of the resonant state, T_1, while the resonance Raman signal is expected to have a lifetime given by the phase-coherence lifetime of the polarization generating the Raman signal, T_2. Because of the large number of ways in which dephasing is possible, T_2 is, in general, much shorter than T_1. In an attempt to conclusively determine whether the observed signals were the result of resonance Raman scattering or fluorescence, lifetime measurements were performed. The $ErPO_4$ crystal was excited at 20 492.9 cm^{-1} in resonance with the transition 0 $cm^{-1} \rightarrow$ 20 492.9 cm^{-1}, and at 20 556.4 cm^{-1} in resonance with the transition from the ground state to one of the two upper crystal-field levels of $^4F_{7/2}$. In both cases, the lifetime of the light emitted at $20\,492.9-33=20\,459.9$ cm^{-1} was measured. The signal excited by radiation at 20 556.4 cm^{-1} is presumed to be fluorescence from population in the level at 20 492.9 cm^{-1} created by fast nonradiative decay of the population at the level at 20 556.4 cm^{-1}. The signal excited by the radiation at 20 492.9 cm^{-1} is either resonance Raman scattering, 0 $cm^{-1} \rightarrow 33$ cm^{-1}, or fluorescence, 20 492.9 $cm^{-1} \rightarrow 33$ cm^{-1}. Both signals were faster than could be measured with a 10-ns pulse as an excitation source, so no determination was possible.

V. RESONANCE RAMAN-EXCITATION PROFILES

The excitation profiles for the $\hat{Y}(\hat{X}\hat{Z})\hat{X}$ Raman-scattering transitions from the ground state to the levels at 33 and 53 cm^{-1} have been measured and the data are plotted as the enhancement of the Raman-scattering intensity versus laser-excitation frequency. The excitation profiles for the $\Delta=33$ cm^{-1} and $\Delta=53$ cm^{-1} electronic Raman scattering for excitation frequencies within ± 25 cm^{-1} from the resonance at 20 492.9 cm^{-1} are shown in Fig. 5. The enhancement of the Raman-scattering intensity is defined as the ratio of the resonance Raman scattering over the nonresonant Raman scattering (not including the ω^4 enhancement). For nonresonant Raman scattering, the excitation used was at 514.5 nm (19 429.7 cm^{-1}), which is at least 300 cm^{-1} from any resonance. In addition, the excitation profile for the vibrational Raman scattering to the 303-cm^{-1} E_g phonon of $ErPO_4$ (Ref. 16) is also shown in Fig. 5. Since there is only a small interaction between the phonons of the crystal and the shielded $4f$ electrons of the rare-earth ion, a resonance excitation of a $4f^N \rightarrow 4f^N$ electronic transition of the rare-earth ion has little or no effect on the vibrational Raman-scattering intensities. Therefore, the vibrational Raman-excitation profiles were used as a standard for comparison with the electronic Raman-scattering profiles. The $\Delta=33$ cm^{-1} and $\Delta=53$ cm^{-1} excitation profiles for excitation frequencies that are 25–100 cm^{-1} less than the resonance frequency are shown in Fig. 6. The $\Delta=303$ cm^{-1} vibrational Raman-excitation profile is not shown because it is approximately flat and equal to 1 in this region.

The excitation profile shown in Fig. 5 for the $\Delta=303$ cm^{-1} vibrational Raman scattering is also flat in the resonance region (reflecting no resonance enhancement as expected) with the exception of a large decrease at approximately 20 493 cm^{-1} and a smaller one at 20 503 cm^{-1}. These decreases are not the result of a variation in the Raman-scattering cross section, but simply reflect the absorption of the incident laser light by the resonant transition 0 $cm^{-1} \rightarrow$ 20 492.9 cm^{-1} and the excited-state transition 53 $cm^{-1} \rightarrow$ 20 556 cm^{-1}. This excited-state absorption is large at such low temperatures because of its large oscillator strength. The absorptions reduce the amount of incident laser light available for Raman scattering in the interior of the crystal, thus resulting in the decreases in the excitation profile.

Excitation profiles for the electronic Raman scattering are dramatically different from the vibrational Raman profile. Both electronic Raman profiles have a double-peaked shape that appears to result from a resonance with two states. The shape actually represents a single resonance structure, however, with a decrease in the center. This decrease is directly "on resonance" and is the result of either absorption of the incident laser beam (as shown in the vibrational Raman-scattering profile) or possibly absorption of the scattered light by population in the final state of the Raman transition. An important feature of both profiles is their asymmetry about the frequency of the resonant transition.

For both profiles the observed enhancements are rela-

tively very large. The peak-enhancement factor is approximately 47 at an excitation 3.0 cm^{-1} from the resonance for the $\Delta=33$ cm^{-1} scattering. The peak-enhancement factor is approximately 141 at an excitation 2.1 cm^{-1} from the resonance for the $\Delta=53$ cm^{-1} scattering. The measured enhancements agree well with results of the earlier experiments that used the 488-nm (20 486.7 cm^{-1}) line of an argon-ion laser as the excitation source (6.2 cm^{-1} from the resonance).[1] In that case the enhancements (relative to excitation at 514.5 nm) were 18.1 and 29.1 for the $\Delta=33$ cm^{-1} and $\Delta=53$ cm^{-1} scattering, respectively. In the present work, measured enhancements for excitation at 488 nm are 18.5 and 28.3 for the $\Delta=33$ cm^{-1} and $\Delta=53$ cm^{-1} scattering, respectively.

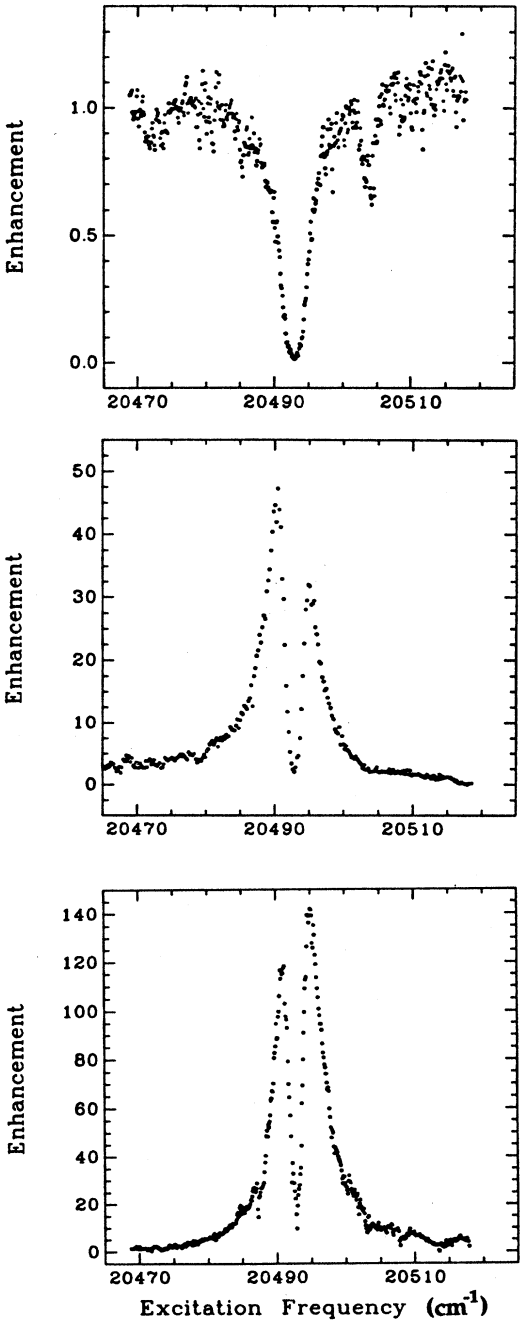

FIG. 5. Top: Excitation profile for the $\Delta=303$ cm^{-1} vibrational Raman scattering. Middle: Excitation profile for the $\Delta=33$ cm^{-1} electronic Raman scattering. Bottom: Excitation profile for the $\Delta=53$ cm^{-1} electronic Raman scattering. For all the cases, the scattering geometry was $\hat{Y}(\hat{X}\hat{Z})\hat{X}$.

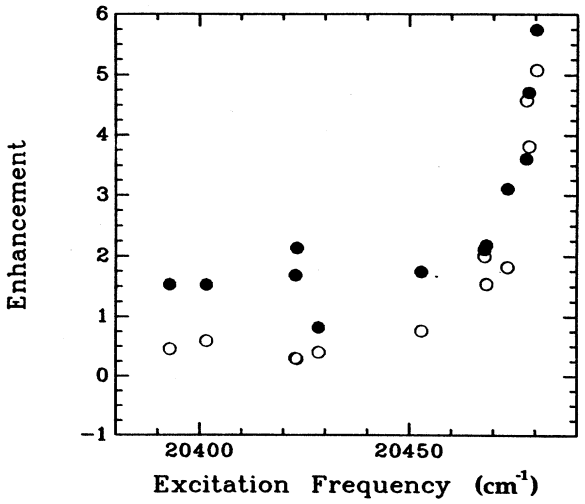

FIG. 6. Excitation profiles for the $\hat{Y}(\hat{X}\hat{Z})\hat{X}$ $\Delta=33$ cm^{-1} and $\Delta=53$ cm^{-1} Raman scattering. Solid circles are for the $\Delta=33$ cm^{-1} scattering. Open circles are for the $\Delta=53$ cm^{-1} scattering.

Electronic Raman-scattering intensities are affected by the resonance for excitation frequencies as far as 100 cm^{-1} off resonance. It can be seen in Fig. 6 that the $\Delta=33$ cm^{-1} scattering is enhanced by a factor of 1.5 relative to the nonresonant scattering (excitation 514.5 nm) for an excitation 100 cm^{-1} lower in energy than the resonance. The $\Delta=53$ cm^{-1} scattering is approximately one-half of the nonresonant scattering for an excitation 100 cm^{-1} lower in energy than the resonance.

VI. MODELING THE EXCITATION PROFILES

The light-intensity associated with an electronic Raman-scattering transition between an initial state $|i\rangle$ and a final state $|f\rangle$ is given by the proportionality

$$(I_s)_{\rho\sigma} \propto \left| \sum_j \left[\frac{\langle f|D_\rho|j\rangle\langle j|D_\sigma|i\rangle}{\omega_j-\omega} + \frac{\langle f|D_\sigma|j\rangle\langle j|D_\rho|i\rangle}{\omega_j+\omega_s} \right] \right|^2 , \quad (1)$$

where ω and ω_s are the frequencies of the incident and scattered light, respectively, D is the electric dipole operator, and ρ and σ are the polarizations of scattered and incident light, respectively. The sum is over the virtual intermediate states $|j\rangle$ (with energy $\hbar\omega_j$) of the Ra-

man process. Because the initial and final states of the Raman transition belong to the ground configuration of the erbium ion ($4f^{11}$), states of the $4f$ configuration do not contribute significantly usually to the sum as virtual intermediate states. Electric dipole matrix elements between states of the same electronic configuration are formally parity forbidden and are only partially allowed in rare-earth crystals through the effect of odd-parity components of the crystal field. In general, states that contribute most significantly as virtual intermediate states belong to the excited configurations of the form $4f^{N-1}n'l$ with parity opposite to that of the ground configuration. If the exciting laser light is sufficiently close in energy to a transition to a state of the $4f^{11}$ configuration, however, the small intraconfigurational electric dipole matrix elements may be offset by the vanishing denominator in Eq. (1), and a $4f^{11}$ state may then contribute non-negligibly as an intermediate state.

The sum in Eq. (1) may be divided into two parts:

$$(I_s)_{\rho\sigma} \propto \left| \sum_{j\neq r} \left[\frac{\langle f|D_\rho|j\rangle\langle j|D_\sigma|i\rangle}{\omega_j-\omega} + \frac{\langle f|D_\sigma|j\rangle\langle j|D_\rho|i\rangle}{\omega_j+\omega_s} \right] + \frac{\langle f|D_\rho|r\rangle\langle r|D_\sigma|i\rangle}{\omega_r-\omega+i\Gamma_r} \right|^2 . \quad (2)$$

The summation includes the nonresonant scattering amplitude (virtual intermediate states are from excited configurations), and the last term arises from the intraconfigurational resonant part of the amplitude. The $4f^{11}$ resonant state $|r\rangle$ has an energy $\hbar\omega_r$. The damping parameter Γ_r has been added to account for the finite lifetime of the polarization that generates the Raman signal. This treatment of the damping factor is only approximate, and a more exact calculation using the density-matrix formalism can be performed.[17,18]

To facilitate the modeling, the following quantities are defined:

$$\Delta\omega=\omega_r-\omega ,$$

$$\eta=|\eta|e^{i\delta} = \frac{\langle f|D_\rho|r\rangle\langle r|D_\sigma|i\rangle}{\sum_{j\neq r}\left[\frac{\langle f|D_\rho|j\rangle\langle j|D_\sigma|i\rangle}{\omega_j-\omega}+\frac{\langle f|D_\sigma|j\rangle\langle j|D_\rho|i\rangle}{\omega_j+\omega_s}\right]} , \quad (3)$$

$$E(\Delta\omega)=\frac{I_s(\Delta\omega)}{I_s^{\text{non-resonant}}} .$$

The quantity η, for the sake of generality, is written as a complex number, and δ is a phase factor. In addition, because of the large energy difference between states contributing to the nonresonant amplitude and the laser excitation, η is assumed to be independent of the laser-excitation frequency. The quantity $E(\Delta\omega)$ is the resonant enhancement of the scattering intensity relative to its nonresonant value.

Using the above definitions and expanding Eq. (2), an expression for the enhancement of the Raman intensity as a function of the frequency ($\Delta\omega$) can be written as

$$E(\Delta\omega)=1+\frac{|\eta|^2}{(\Delta\omega)^2+\Gamma_r^2}+\frac{2|\eta|\Gamma_r\sin\delta}{(\Delta\omega)^2+\Gamma_r^2} + \frac{2|\eta|\Delta\omega\cos\delta}{(\Delta\omega)^2+\Gamma_r^2} . \quad (4)$$

The right-hand side of this expression may be divided into three parts. The first term represents the contribution from the nonresonant amplitude. The second term is the contribution from the resonant amplitude. The third part, which consists of the third and fourth terms, results from interference between the nonresonant and resonant amplitudes. Note that the first three terms are symmetric in $\Delta\omega$, but the last term is antisymmetric. Thus, the summation of all terms yields an asymmetric profile as experimentally observed.

It is necessary to include effects of inhomogeneous broadening of the resonant transition to complete this model. For any given laser frequency, the value of $\Delta\omega$ varies from erbium ion to erbium ion throughout the crystal. To account for this variation, Eq. (4) for $E(\Delta\omega)$ is summed over the distribution of possible resonant energies in the crystal. A Gaussian distribution (the absorption spectra indicate that this is an appropriate choice[19]) is assumed of the form

$$S(\Delta\omega')=\frac{2}{\Delta}\left[\frac{\ln 2}{\pi}\right]^{1/2}\exp\left[-\left[4\ln 2\frac{(\Delta\omega')^2}{\Delta^2}\right]\right] , \quad (5)$$

where Δ is the FWHM of the Gaussian, and $\Delta\omega'$ is the detuning from the mean frequency of the Gaussian. Absorption spectra of $ErPO_4$ crystals show that Δ for the transition 0 $cm^{-1}\rightarrow$20 492.7 cm^{-1} is approximately 2 cm^{-1}, as noted before. E is summed over the inhomogeneous profile in the integral

$$E(\Delta\omega)=\int_{-\infty}^{\infty} E(\Delta\omega-\Delta\omega')S(\Delta\omega')d(\Delta\omega') . \quad (6)$$

This model does not include the effect of absorption of the exciting laser light by the resonant transition. This effect was factored out of the observed electronic Raman-excitation profiles by dividing these profiles by the excitation profile for the $\Delta=303$ cm^{-1} vibrational Raman transition. The model was then fitted to these "normalized" profiles. For each profile, values of $|\eta|$ and δ which yielded the best fits to the observed profiles were selected. The damping parameter Γ_r is given by the homogeneous width of the resonant transition. Since the linewidth of the resonant transition is approximately 2 cm^{-1} (most of this linewidth is attributed to inhomogeneous broadening), an upper limit of 2 cm^{-1} may be set on the value of Γ_r. A lower limit for the linewidth is given by the finite linewidth of the exciting-laser line, 0.25 cm^{-1}. From Eq. (4) it can be seen that the results of the model are fairly insensitive (with $|\eta|\gg\Gamma_r$ and $\Delta\omega\gg\Gamma_r$) to the value of Γ_r. (The magnitude of Γ_r only becomes important when the laser is tuned into direct resonance, where it is strongly absorbed. Under these conditions, a

comparison between the data and the model is not possible.) Thus Γ_r was fixed at 0.4 cm^{-1} for the fits.

The best fits to the excitation profile are given by $|\eta|=22$ and $\delta=\pi/3$ and $|\eta|=35.5$ and $\delta=2\pi/3$ for the $\Delta=33$ cm^{-1} and $\Delta=53$ cm^{-1} transitions, respectively. The observed and calculated profiles for the $\Delta=33$ cm^{-1} and $\Delta=53$ cm^{-1} scattering are shown in Fig. 7 for laser-excitation frequencies within ± 25 cm^{-1} of the resonance. In Fig. 8 the same profiles are shown for laser-excitation frequencies in the region 25–100 cm^{-1} below the resonance. Both fits accurately describe the magnitudes and shapes of the excitation profiles.

The value of $|\eta|$ associated with a given process may be calculated from Eq. (3) if the nonresonant amplitude of the Raman transition and the electric dipole matrix elements for the initial-state to resonant-state and resonant-state to final-state transitions are known. The magnitude of the electric dipole matrix element may be obtained directly from the value of the oscillator strength of the associated one-photon transition (the oscillator strength of a transition is proportional to the magnitude of the electric dipole matrix element squared). The oscillator strengths of the crystal-field transitions between the $^4I_{15/2}$ multiplet and the $^4F_{7/2}$ multiplet were measured from absorption spectra and are listed in Table I. The relative values of the nonresonant amplitudes of the electronic Raman scattering have been given previously.[16] Thus, the relative values of $|\eta_{33}|$ and $|\eta_{53}|$ may be calculated. From Eq. (3) we have

$$\frac{|\eta_{33}|}{|\eta_{53}|}=\frac{\left|\dfrac{\langle 33|X|r\rangle\langle r|Z|0\rangle}{\mathcal{A}_{33}}\right|}{\left|\dfrac{\langle 53|X|r\rangle\langle r|Z|0\rangle}{\mathcal{A}_{53}}\right|}, \tag{7}$$

where $|r\rangle$ is the resonant state at 20 492.9 cm^{-1} and $\mathcal{A}_{33}$ and $\mathcal{A}_{53}$ are the nonresonant Raman amplitudes for the $\Delta=33$ cm^{-1} and $\Delta=53$ cm^{-1} scattering. From Table I and the relative nonresonant Raman amplitudes[16] ($\mathcal{A}_{33}/\mathcal{A}_{53}=1.82$), we find, from Eq. (7),

$$\frac{|\eta_{33}|}{|\eta_{53}|}=0.58\ . \tag{8}$$

This value is in excellent agreement with the ratio ob-

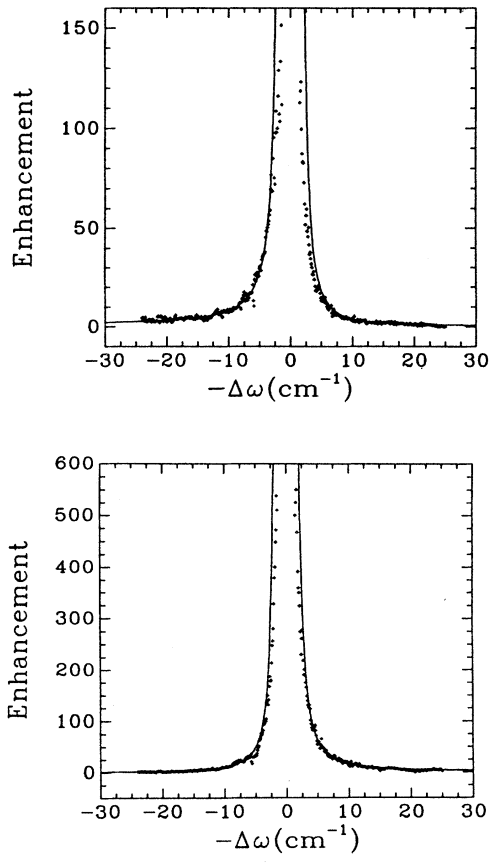

FIG. 7. Measured and modeled "normalized" Raman-excitation profiles for the $\hat{Y}(\hat{X}\hat{Z})\hat{X}$ $\Delta=33$ cm^{-1} and $\Delta=53$ cm^{-1} transitions. The top panel is for the $\Delta=33$ cm^{-1} transition, the bottom for the $\Delta=53$ cm^{-1} transition.

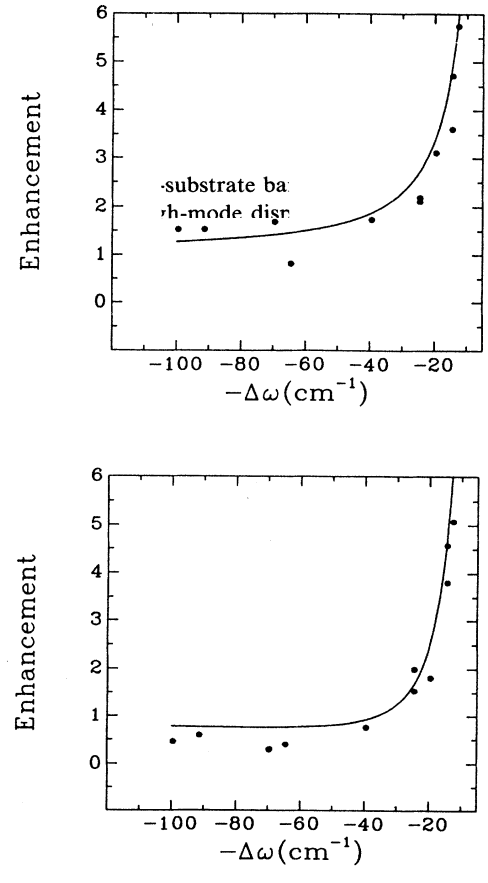

FIG. 8. Measured and modeled "normalized" Raman-excitation profiles for the $\hat{Y}(\hat{X}\hat{Z})\hat{X}$ $\Delta=33$ cm^{-1} and $\Delta=53$ cm^{-1} transitions. The top panel is for the $\Delta=33$ cm^{-1} transition, the bottom for the $\Delta=53$ cm^{-1} transition.

TABLE I. Oscillator strengths for transitions between the crystal-field levels of the $^4I_{15/2}$ and $^4F_{7/2}$ multiplets in $ErPO_4$.

Transition	Energy (cm^{-1})	Polarization	Oscillator strength ($\times 10^6$)
0 cm^{-1}→20492.9 cm^{-1}	20492.9	$\hat{X}=\hat{Y}$	0.092
		$\hat{Z}$	0.069
0 cm^{-1}→20485.0 cm^{-1}	20485.0	$\hat{X}=\hat{Y}$	0.003
		$\hat{Z}$	not allowed
33 cm^{-1}→20492.9 cm^{-1}	20459.9	$\hat{X}=\hat{Y}$	0.760
		$\hat{Z}$	not allowed
33 cm^{-1}→20485.0 cm^{-1}	20452.0	$\hat{X}=\hat{Y}$	0.187
		$\hat{Z}$	0.020
53 cm^{-1}→20492.9 cm^{-1}	20439.9	$\hat{X}=\hat{Y}$	0.671
		$\hat{Z}$	0.011
53 cm^{-1}→20485.0 cm^{-1}	20432.0	$\hat{X}=\hat{Y}$	0.148
		$\hat{Z}$	not allowed

tained from the fitted values of $|\eta|$:

$$\left[\frac{|\eta_{33}|}{|\eta_{53}|}\right]_{\text{fitted}}=\frac{22}{35.5}=0.62\ . \tag{9}$$

The oscillator strength for the transition from the ground state to the resonant state is relatively small, yet the oscillator strengths for the transitions from the resonant state to the final states are both relatively quite large (Table I). The latter two oscillator strengths are nearly 1×10^{-6}, i.e., the same magnitude as a typical multiplet-to-multiplet oscillator strength. It is this combination of a small initial- to resonant-state oscillator strength and a large final- to resonant-state oscillator strength that will, in general, result in large observable resonances in electronic Raman scattering and other two-photon processes in rare-earth crystals. This combination minimizes absorption losses of the exciting laser light, while maintaining the product of the matrix elements that determine the strength of the Raman scattering.

The second parameter in the model is the phase δ as defined in Eq. (3). From Eq. (3), δ might be expected to have a value of 0 or π, indicating either complete constructive or destructive interference between the resonant and nonresonant amplitudes. The best fits of the observed excitation profiles were given by $\delta_{33}=\pi/3$ and $\delta_{53}=2\pi/3$. These values were necessary in order to accurately match the symmetric part with the antisymmetric part of the profiles. It is difficult to justify these phases on physical grounds. The fact that δ is not necessarily 0 or π, however, has two important implications. First, the tuning range over which the resonance is observable is reduced. From Eq. (4) it can be seen that the interference term controls the range of the resonance and drops off only as $1/\Delta\omega$, while the resonant term drops off as $(1/\Delta\omega)^2$. The size of the interference term is dependent on the factor $\cos\delta$. Thus, the greatest range of resonance effects is attained for values of δ and 0 or π. Second, there is no complete or even near cancellation of the Raman signal at a given value of $\Delta\omega$. Equation (4) shows that for $\delta=0$ or π the Raman signal will almost completely vanish (assuming $\eta\gg\Gamma$) for an excitation frequency of $\Delta\omega\approx-\eta$ or η, respectively, but, in fact, no cancellation of the Raman scattering has been observed.

VII. CONCLUSIONS

The previously reported observation[1] of a large intraconfigurational intermediate-state resonance enhancement of electronic Raman scattering in $ErPO_4$ has been confirmed. Excitation profiles for the resonance enhancement were obtained, and the shapes and magnitudes of these profiles were accurately modeled using standard theory. The results of this modeling indicate that the optimum conditions for the observation of large intermediate-state resonance enhancements of electronic Raman scattering are a small oscillator strength for the initial-state to resonant-state transition, combined with a large oscillator strength for the final-state to resonant-state transition.

ACKNOWLEDGMENTS

We acknowledge very helpful discussions with J. Arnold Koningstein, Rufus Cone, Michael Reid, and David Piehler. We thank Jin Huang, G. K. Liu, and Rufus Cone for supplying us with a copy of their article on resonant enhancement of two-photon absorption, prior to publication. This research was supported in part by the Director, Office of Energy Research, Office of Basic Energy Sciences, Chemical Science Division, U.S. Department of Energy, under Contract No. DE-AC03-76SF00098. Oak Ridge National Laboratory is operated by Martin Marietta Energy Systems, Inc., for the U.S. Department of Energy under Contract No. DE-AC05-84OR21400.

*Present address: Naval Research Laboratory, Washington, D. C. 20375-5000.

†Present address: AT&T Bell Laboratories, Murray Hill, NJ 07974-2070.

[1]P. C. Becker, G. M. Williams, R. E. Russo, N. Edelstein, J. A. Koningstein, L. A. Boatner, and M. M. Abraham, Opt. Lett. **11**, 282 (1986).

[2]R. L. Wadsack and R. K. Chang, Solid State Commun. **10**, 45 (1972).

[3]D. Nicollin and J. A. Koningstein, Chem. Phys. **49**, 377 (1980).

[4]P. Myslynski and J. A. Koningstein, Chem. Phys. **114**, 137 (1987).

[5]R. L. Cone, D. A. Ender, M. S. Otteson, P. L. Fisher, J. M. Friedman, and H. J. Guggenheim, in *Laser Techniques for Extreme Ultraviolet Spectrocopy, Subseries on Optical Science and Engineering Number 2,* Proceedings of the Topical Meeting on Laser Techniques for Extreme Ultraviolet Spectroscopy, AIP Conf. Proc. No. 90, edited by T. J. McIlrath and R. R. Freeman (AIP, New York, 1982), p. 471.

[6]R. L. Cone, D. A. Ender, M. S. Otteson, P. L. Fisher, J. M.

Friedman, and H. J. Guggenheim, Appl. Phys. B **28**, 143 (1982).
[7]D. A. Ender, M. S. Otteson, R. L. Cone, and H. J. Guggenheim, Opt. Lett. **7**, 611 (1982).
[8]D. A. Ender, M. S. Otteson, R. L. Cone, and H. J. Guggenheim (unpublished).
[9]D. A. Ender, M. S. Otteson, R. L. Cone, and H. J. Guggenheim (unpublished).
[10]J. Huang, G. K. Liu, R. L. Cone, Phys. Rev. B **39**, 6348 (1989).
[11]W. O. Milligan, D. F. Mullica, G. W. Beall, and L. A. Boatner, Inorg. Chim. Acta. **60**, 39 (1972).
[12]Philippe C. Becker, Ph.D. thesis, University of California, Berkeley, 1986.
[13]P. F. Williams, D. L. Rousseau, and S. H. Dworetsky, Phys. Rev. Lett. **32**, 196 (1974).
[14]Y. Masumoto, S. Shionoya, and Y. Tanaka, Solid State Commun. **27**, 1117 (1978).
[15]J. S. Weiner and P. Y. Yu, Solid State Commun. **50**, 493 (1984).
[16]P. C. Becker, N. Edelstein, G. M. Williams, J. J. Bucher, R. E. Russo, J. A. Koningstein, L. A. Boatner, and M. M. Abraham, Phys. Rev. B **31**, 8102 (1985).
[17]Y. R. Shen, Phys. Rev. B **9**, 622 (1974).
[18]D. Lee and A. C. Albrecht, in *Advances in Infrared and Raman Spectroscopy,* edited by R. J. H. Clark and R. E. Hester (Wiley, New York, 1985), Vol. 12.
[19]Glen M. Williams, Ph.D. thesis, University of California, Berkeley, 1988.